Journal of Applied Sciences and Nanotechnology

Journal homepage: jasn.uotechnology.edu.iq

Synergistic Effect of Acacia (*Cassia siamea*) Leaves Extract in Green Synthesis of Ag/TiO_2 Nanostructures for Dye-Sensitized Solar Cells

[1]Joseph Adegbite Adebanji, [1]Gabriel Ayinde Alamu, [2]Khadijat Kuburat Babalola, [3]Ayodele Joshua Abiodun, [4]Oludele Adegboyega, [1]Hakeem Olayinka Oyeshola, [1,5]Oluwaseun Adedokun*, [1,5]Yekinni Kolawole Sanusi

[1]*Department of Pure and Applied Physics, Ladoke Akintola University of Technology, Ogbomoso, Nigeria*
[2]*Department of Physical and Chemical Sciences, Federal University of Health Sciences, Ila-Orangun, Nigeria*
[3]*Department of Physics, Lead City University Ibadan, Oyo Nigeria*
[4]*Department of Physics, Emmanuel Alayande University of Education, Oyo, Nigeria*
[5]*Nanotechnology Research Group (NANO+), Ladoke Akintola University of Technology, Ogbomoso, Nigeria*

ARTICLE INFO

Article history:
Received: April, 28, 2025
Accepted: December, 05, 2025
Available online: December, 10, 2025

Keywords:
Green synthesis,
Ag/TiO_2 nanostructures,
Photoanode,
Power conversion efficiency,
Dye-sensitized solar cells

Corresponding Author:
Oluwaseun Adedokun
oadedokun@lautech.edu.ng

ABSTRACT

The green-synthesized silver-titanium dioxide (Ag/TiO_2) nanocomposite was successfully produced in this study by the synergistic effects of the *Cassia siamea* leaf extract. In the visible portion of the electromagnetic spectrum, the absorbance improved when the nanoparticle was incorporated into TiO_2. The energy gap of the composite reduced as the absorbance increased. Numerous functional groups in the formation of NP were detected by FTIR, and their possible role in NP formation was suggested. The synthesized nanoparticles and nanocomposites were found to be crystalline with X-Ray Diffraction (XRD) studies. The average crystallite size of the nanoparticle was 3.95 nm compared to nanocomposite of 4.53 nm. The shape of the surface of the synthesized nanocomposite appeared smoother and spherical in the scanning electron microscopy (SEM) image. The Energy Dispersive Spectra (EDS) of the TiO_2 nanocomposite confirmed the existence of Ag and other elements. The formation of nanoparticles and nanocomposites having an average size of 4.85 nm and 6.92 nm was also verified on the basis of the analysis of the particles' TEM micrographs. The incorporation of silver nanoparticles (AgNPs) increased the conductivity by 60.24% and resulted in promising electrical properties that suggest their potential application in a dye-sensitized solar cell (DSSC).

https://doi.org/10.53293/jasn.2025.7620.1343, Department of Applied Sciences, University of Technology - Iraq.

1. Introduction

A dye-sensitized solar cell (DSSC) is a type of photovoltaic technology that generates electricity from light and mimics the natural process of photosynthesis. A DSSC is constituted by an electrolyte, a counter electrode, and a photoanode, which absorbs the energy of a photon by a dye molecule. To work as a DSSC, charge separation also needs to be achieved such that electrons transferred from the excited dye molecules are injected into the conduction band of the photoanode material. These electrons are carried by a wire to an external circuit to generate electricity. Despite its potential, the overall performance of dye-sensitized solar cells (DSSCs) is limited by factors such as the dye's light absorption capacity, the surface area of the photoanode, and the rate of charge recombination. To enhance the performance of the DSSC photoanode, many DSSC photoanode

composite materials have been proposed by adding nanomaterials, which can enhance e-transport, CS and light harvesting [1].

The development of complex nanomaterials to boost the performance of DSSC has been widely studied. Among such materials, Ag-titanium dioxide (Ag/TiO_2) nanostructures have attracted particular interest due to the synergism of a high surface area, plasmonic effect, and photocatalytic activity. In the past few years, nanocomposites, especially nanocomposites of noble metals (e.g., Ag) and semiconductors (e.g., TiO_2), have gained extensive interest in advanced materials due to their extraordinary optical, electrical, and catalytic properties. Ag/TiO_2 nanocomposites integrate the plasmonic properties of AgNPs and the semiconducting properties of TiO_2. AgNPs possess special optical properties, known as surface plasmon resonance (SPR), which may lead to an increase in light harvesting or reduce the recombination of electron-hole pairs, as well as promote the charge transfer. These properties make Ag an excellent candidate for enhancing solar cell efficiency. Yet, TiO_2 is a semiconductor well employed in DSSC for its high specific area, its chemical resistance and its contribution to the electron transfer. It is expected that introducing AgNPs into the TiO_2 matrix can improve the efficiency of charge separation and photoelectric performance. Due to their synergistic effects, nanocomposites of Ag and TiO_2 have been considered to be suitable for enhancing the performance of DSSCs [2, 3].

Classic Ag/TiO_2 nanocomposites preparation practices are usually restricted to the application of hazardous reagents, high temperature and complications of the treatment. On the other hand, green synthesis procedures, which employ biogenic materials such as plant extracts, possess several merits, including biocompatibility, eco-friendliness, ease of use, low cost, environmental sustainability, and minimal generation of hazardous waste. The green synthesis approach employing ecologically friendly methods and plant extracts is a green alternative method to traditional chemical methods for the fabrication of these nanocomposites. Plant extracts contain bioactive substances (i.e., polyphenols, flavonoids, alkaloids, and terpenoids) as reductants of metal ions and as stabilizers of the nanoparticles. These materials may also act as capping agents that prevent the aggregation of nanoparticles and increase their stability [4, 5]. For example, Hamid et al. (2025) investigated antibacterial and antibiofilm potentials of AgNPs prepared by *Carthamus tinctorius* extract against several MDR bacterial strains. The work aimed to develop a greener and improved method of AgNPs synthesis and to evaluate its antimicrobial properties against the multidrug-resistant biofilm-forming bacteria. Several characterization techniques (UV–visible spectroscopy, SEM, TEM, FTIR, EDS) have been employed to verify the spherical AgNPs that were obtained in the size range of 20–60 nm through biosynthesis. The antimicrobial activity of the biosynthesized AgNPs was also investigated. All data suggested the potentiality of applying AgNPs as bioactive against bacterial infection, biofilm, and drug-resistant bacteria in biotechnology and pharmacology. The potential of *C. tinctorius* AgNPs for the development of antimicrobials became evident from the survey [6]. Acacia leaves (*C. siamea*), citrus peel extract, and green tea extract have also been utilized to produce AgNPs. Similarly, eco-friendly synthesis of TiO_2 NPs can be accomplished with plant extracts. Combining these methods enables the synthesis of Ag/TiO_2 nanocomposites with improved plasmonic and photocatalytic characteristics, leading to enhanced performance in dye-sensitized solar cells (DSSCs). [4].

Recently, the production of AgNPs from the leaves of the acacia plant has been receiving obvious attention as it has several advantages. Due to the vast variety of phytochemicals present in the plant, this can serve as a greener substitute on an industrial scale for chemical and physical procedures applied for the synthesis of nanoparticles. This approach is environmentally friendly since the carbon footprint is minimized and the generation of hazardous waste is avoided. Furthermore, greener nanotechnology involving the use of natural resources for the production of nanomaterials that are environmentally and ecologically safe is referred to as sustainable nanotechnology. Because acacia trees are widely and commonly found everywhere, particularly in arid and semi-arid areas, the preparation of nanoparticles from their leaf extracts can be an environmentally friendly and potentially renewable resource in support of a greener environment. Moreover, the use of plant extracts, especially acacia leaf, for the synthesis of AgNPs is cost-effective. Acacia leaves-based AgNPs could serve as an economical source for large-scale production of AgNPs as they are accessible, easy to collect and do not involve the use of expensive chemicals. It is very easy to prepare the nanoparticles, which can be made without the need for any complex steps, except for the required reagents. Implication of the study: Acacia leaves were extracted in a simple way that involves only crushing the leaves, boiling to extract active compounds and mixing with silver

nitrate ($AgNO_3$) solution. Its simplicity renders it inexpensive and applicable to resource-poor settings where access to more complex chemical methods might be limited [7].

Two important advantages of the production of AgNPs from acacia plant leaves are their biocompatibility and low toxicity. Furthermore, phytochemicals present in the acacia leaves extract compound stabilize the AgNPs from causing harm to live organisms. This is particularly relevant given that toxicity is one of the predominant issues influencing the use of QD in biomedical applications [8]. Furthermore, the process to fabricate AgNPs utilizing plant extract such as acacia leaves allows for the controlled synthesis of NPs of specific size and shape. The size and shape of NPs are essential factors affecting the physical, chemical, and biological properties of nanoparticles. The particle size of these A cohenii leaf-reduced silver nanoparticles was also reported to be in the range of 30 and 40 nm [9]. This smaller size region is of particular interest for a wide range of applications since smaller NPs have a higher surface area-to-volume ratio that enhances their reactivity and performance [10]. The presence of phytochemicals in the acacia extract can serve as natural templates for shaping nanoparticles with controlled morphology, thus facilitating a broad range of nano-fabrication [11].

One of the pioneers in this field was Murugan et al. (2014) biosynthesized environmentally benign AgNPs by employing chloroform-mediated A. leucophloea leaf extract. This research showed the inherent reducing potential of flavonoids and polyphenolic compounds found in acacia leaf extracts. The chemicals that were found in the acacia leaf starch reduction process in the $AgNO_3$ solution were used as an $AgNO_3$ pregnant solution. The resulting AgNPs had antibacterial activity and highly efficient bactericidal activity against several Gram-positive and negative bacteria. This report demonstrated the environmental friendliness of the synthesis process and recommended the use of acacia leaf extract as an eco-efficient approach for the production of AgNPs for potential applications on antimicrobial coatings and wound healing, and the treatment of water [12].

Edwina et al. (2020) successfully reduced the silver ions of aqueous A. Senegal leaf extract into AgNPs using the process of bioreduction of $AgNO_3$ solution. The resultant AgNPs were well dispersed with mean particle sizes ranging between 10 and 19 nm, suitable for antibiotic testing. The FTIR spectra of AgNPs and leaf extract revealed strong broad band peaks, which are probably one that provided the effective stabilization and capping to the AgNPs. In a similar way, production of similar or different metallic nanoparticles that are bactericidal for a range of biological applications may be easily scaled up in industry by this method [13].

AgNPs were synthesized by the green method as reported by Nuha and co-workers (Nuha et al., 2023) for chemoresistant cancer cells and bacteria. A significant peak in SPR at 375 nm confirmed the existence of AgNPs. The polydispersity index was 0.297, and the Z-average size was 105.4 nm. TEM revealed particle sizes ranging from 11 to 30 nm. The generated AgNPs had a cytotoxic effect on cancer cell lines and demonstrated promising antibacterial effectiveness against bacterial strains. Every gene's expression levels changed after being treated with extract and AgNPs. This study [14] revealed that both *A. nilotica* pods and *A. nilotica*-AgNPs are promising possibilities for antibacterial and anticancer usage.

Ibrahim *et al.* (2024) made great efforts to use *A. raddiana* leaf extract as a stabilizing and reducing agent in the ecologically friendly production of AgNPs. The XRD measurements showed the production of AgNPs with crystallite sizes ranging from 20-30 nm. According to SEM and TEM examinations, the AgNPs are generally spherical or rod-shaped, with sizes ranging from 8 to 41 nm. Importantly, at 70 °C and the basic conditions (pH 10), the rate of AgNPs generation increased significantly. These findings show that *A. raddiana* works well as a feedstock for the manufacture of sustainable AgNPs. It demonstrates the promise of *A. raddiana* in the environmentally friendly production of AgNPs and their efficacy as environmental sensors for heavy metals [15].

The extract from acacia leaves has demonstrated remarkable synergistic prospective in a variety of sectors for a wide range of applications. Therefore, this innovative study investigated the remarkable possibilities of *C. siamea* leaf extract in the environmentally friendly production of Ag/TiO_2 nanostructure and its use to improve the DSSC photoanode's effectiveness. The Ag/TiO_2 nanostructures were produced using fresh acacia leaf extract,

and data analysis using UV–vis spectroscopy, FTIR, XRD, SEM, EDS, and TEM were performed. The four-point probe technique was used to electrically characterize TiO_2 and modified TiO_2 films.

2. Materials and Methods

2.1. Materials

Sigma-Aldrich's TiO_2 (P25) and $AgNO_3$ were utilized without additional purification. Fresh acacia leaves were gathered from the Forestry Research Institute of Nigeria (FRIN) in Jericho, Ibadan, Nigeria. Non-conducting glass slides, Whatman filter papers, ethanol, distilled water, and Isopropanol acid (IPA) were bought from XIN Yan Technology Limited in China.

2.2. Green Synthesis of AgNPs

The Forestry Research Institute of Nigeria (FRIN) in Jericho, Ibadan, provided the fresh acacia (*C. siamea*) leaves (**Fig. 1a**). The leaves were collected in the morning, before the heat of the day, to preserve delicate compounds. The fresh acacia leaves were cleaned with distilled water and left to air dry. After being dried, the leaves were ground and sieved into a fine powder and stored in a clean and dry container. The powder (20 g) was boiled with 1 liter of deionized water at 60 °C for 30 minutes, and its extract was filtered using Whatman No. 1 filter paper [2]. 0.017 g of $AgNO_3$ and 100 mL of distilled water were combined to create an $AgNO_3$ solution (1 mM). The extract was then added individually to the ($AgNO_3$) solution (10 mL of 1 mM $AgNO_3$) to create AgNPs (2 mL, 4 mL, 6 mL, 8 mL, and 10 mL). To optimize the extract volume required for the synthesis of AgNPs, various sample volumes were tested (**Fig. 1b**).

Figure 1: (**a**) *C. siamea* leaves, (**b**) Synthesized AgNPs at different volumes of *C. siamea* leaves extract

2.3. Deposition of Films

TiO_2 powder weighing 1.0 g was placed in a sterile beaker. The aggregates were broken up into separate particles by adding 2.5 mL of distilled water. 0.5 g of ethyl cellulose was dissolved by mixing the substance with 50 mL of ethanol. The mixture was then placed on the magnetic stirrer after adding 5 mL of terpineol. The mixture was then heated to 60 °C while being agitated for an hour in order to produce a uniform paste, with 50 mL of ethanol added at regular intervals. To further optimize the volume needed for an increased photoanode in DSSC, different volume fractions of the optimized AgNPs for film fabrication (0.5 mL, 1.0 mL, 1.5 mL, and 2.0 mL) were combined with the paste. The glass substrates were ultrasonically cleansed in a water bath of distilled water for 15 minutes at 30 °C after being cleaned with a detergent solution. IPA was then used to clean the substrates for 30 minutes at 30 °C in an ultrasonic bath. In order to control the regions of the films and offer uncoated areas for electrical contact, the glass substrates were initially wrapped with adhesive tape on two parallel edges. A glass rod was used to disseminate the produced pastes after they had been applied to one edge of the cleaned glass substrates. A reference electrode devoid of nanoparticles was also made. After relaxing for a few minutes to lessen surface imperfections, the films were dried at 125 °C for 15 minutes. Electrical and optical characterizations were then performed [16]. The film samples that were applied to the glass substrates are displayed in **Fig. 2**.

Figure 2: Deposited films

2.4. Characterizations

The optical absorptions were examined using the UV-Vis spectrometer (ASUV-6300PC for the nanoparticles and Avantes model Avalight DH 5 BAL for the films), and the FTIR spectrophotometry was examined using the NICOLET iS10 spectrometer. A scanning electron microscope (JOEL-JSM 7600F) was used to characterize the films' morphology, while a Rigaku D/Max-IIIC X-ray diffraction apparatus was used to determine the crystallographic structure. TEM analysis was performed using a JEM-ARM200F-G TEM equipment to analyze the morphologies and particle sizes of the nanoparticles, TiO_2, and modified TiO_2. To measure electrical qualities, a four-point probe (KEITHLEY instrument, 6220DC current source) was employed.

3. Results and discussion

3.1. Optical Studies

3.1.1. Optical Absorbance of the Synthesized AgNPs

To find the ideal amount of leaf extract to combine with $AgNO_3$ to produce AgNPs, the samples were optically characterized using a Jewry 6405 UV-Vis spectrophotometer. **Fig. 3** depicts the UV-Vis optical absorptions of AgNPs generated with different concentrations of *C. siamea* leaf extract as a reducing agent. A 10mL of a 1mM $AgNO_3$ solution was mixed with different volumes (2–10 mL) of leaf extract to synthesize silver nanoparticles (AgNPs). Production of AgNPs was assessed by gradual color alteration of the reaction medium from a brown to yellowish-brown color due to excitation of silver nanoparticles (AgNPs), this consequence is most likely attributed to surface plasmon resonance (SPR) related with Ag nanoparticles behavior [17].

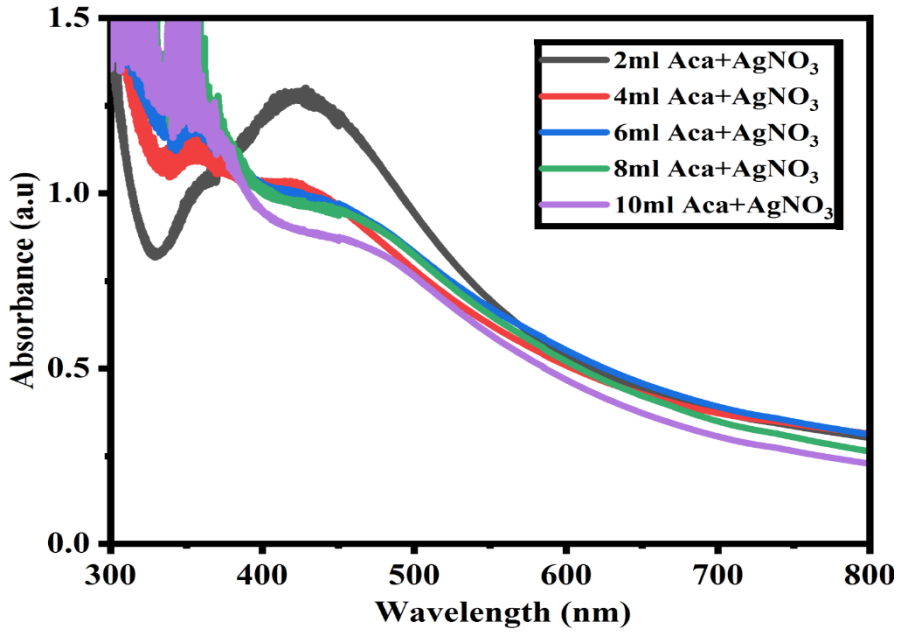

Figure 3: Optical absorbance of AgNPs synthesized with different volumes of *C. siamea* leaves extract

The strong yellow brown color was an indication of the successful synthesis of nanoparticles. UV-Vis analysis demonstrated an absorption peak of the SPR vibration at 425nm, indicating that Ag NPs were effectively synthesized [18]. An increase in the leaf extract volume caused a decrease in the intensity of absorption and a red shift of the SPR band, indicating that AgNPs can be produced with minimum extract [18]. Visual and spectral analysis showed that 2 mL of extract with 10 mL of 1 mM $AgNO_3$ solution was sufficient to produce well-formed AgNPs, with a peak around 425 nm. These nanoparticles were later used for thin film deposition.

3.1.2. Optical Absorbance of TiO_2 Thin Films with AgNPs

Fig. 4 shows the UV-Vis optical absorption of TiO_2 film samples with and without the synthesized AgNPs. The optimized nanoparticles also varied (0.5 mL, 1.0 mL, 1.5 mL, and 2.0 mL) using the same volume (1.0 mL) of the TiO_2 paste. Due to its wide band gap, the TiO_2 paste without nanoparticles did not exhibit any absorbance in the visible region, as seen in **Fig. 4**. Combining AgNPs with the paste affected the absorbance in the visible spectrum because of the SPR band of the AgNPs [19]. The sample containing 2 mL of the optimized nanoparticle had the highest evident absorption and was used for further characterizations.

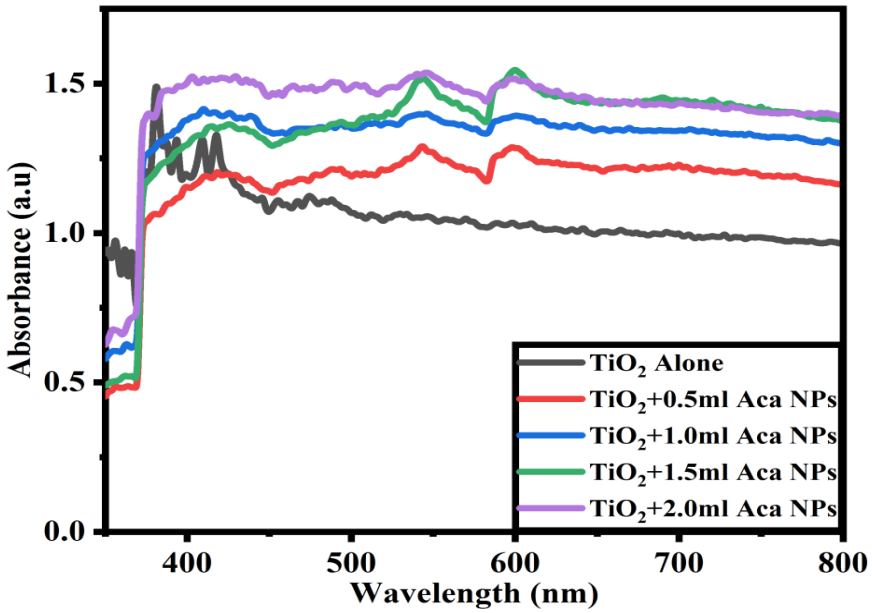

Figure 4: Optical absorbance of TiO_2 and modified TiO_2 films

3.1.3. Optical Band Gap

The films' optical band gaps were determined by plotting $(\alpha hv)^2$ vs. hv curves. The energy band gaps were calculated using a straight-line plot of $(\alpha hv)^2$ vs hϋ and projecting it to the baseline. **Fig. 5** shows the optical band gaps for TiO_2 paste combined with AgNPs derived from *C. siamea* leaf extract. It was observed that the TiO_2 film containing 0.5 mL of the nanoparticle has an estimated energy gap of 2.38 eV, while the film containing 1.0 mL had an energy gap of 2.23 eV. The energy gap of the film with 1.5 mL of the nanoparticle is 2.18 eV, while that of the film with 2.0 mL of the nanoparticle is 2.05 eV. This graph shows that as the nanoparticle concentration increased, the band gap reduced.

The data, shown in **Table 1**, indicate that as absorbance increased, the energy gap decreased. This proves that as nanoparticle concentration increased, the distance between the particles decreased, leading to enhanced interactions and reduced quantum confinement effects. Increased concentration can also result in stronger particle-particle interactions, influencing the electronic structure and reducing the energy gap. Because electrons require less energy to flow through the material's Fermi level, a smaller energy gap indicates increased conductivity [20]. Lowering the optical band gap in TiO_2 films is critical for their photocatalytic activity because it results in increased light absorption, a larger population of excited electrons, and more successful catalytic

processes [21]. As a result, lowering the film's bandgap increases electron transport to the TiO_2 conduction band, hence enhancing the efficiency of the TiO_2 photoanode [20].

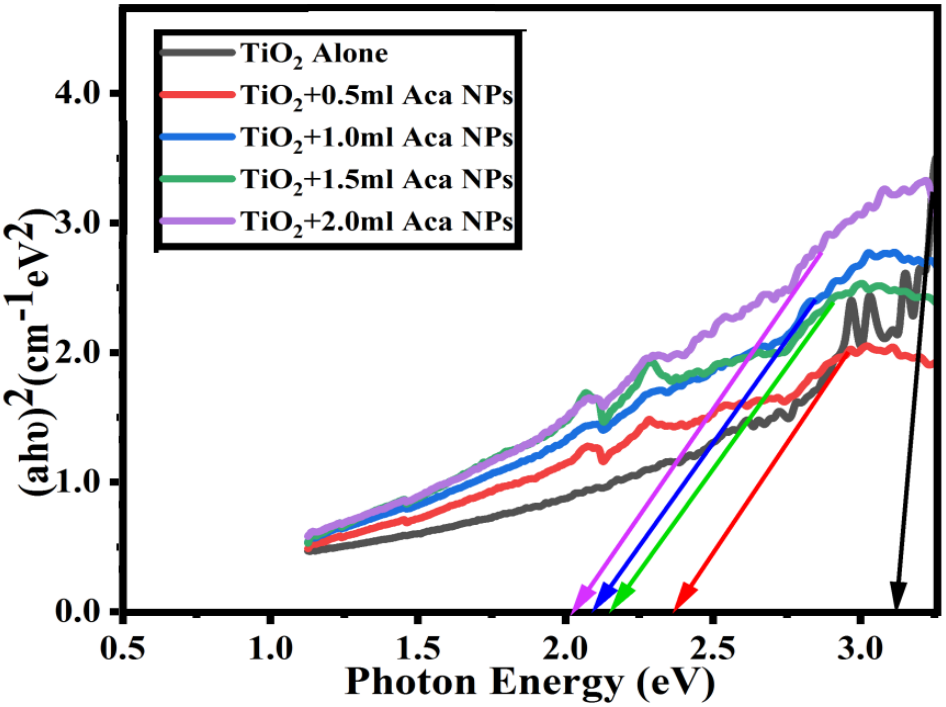

Figure 5: Optical band gap of the TiO_2 films incorporated with the synthesized AgNPs

Table 1: Optical band gap of the TiO_2 films incorporated with the synthesized AgNPs

Sample	Energy gap (eV)
TiO_2 film	3.25
TiO_2 @ 0.5 mL nanoparticle	2.38
TiO_2 @ 1.0 mL nanoparticle	2.23
TiO_2 @ 1.5 mL nanoparticle	2.18

3.2. FTIR Spectroscopy of AgNPs

The FTIR spectra of the AgNPs synthesized using the *C. siamea* leaf extract are shown in **Fig. 6**. The spectra also revealed the functional groups and their possible contribution to the nanoparticles' formation. From **Fig. 6**, the IR band observed at 683.13 cm^{-1} in the extract is attached to the strong disubstituted C=C bending of alkane compound; 778.34 cm^{-1} to medium trisubstituted C=C bending of alkane compound; 1054.09 cm^{-1} to strong C-O stretching of primary alcohol; 1630.66 cm^{-1} to medium C=C stretching of conjugated alkene compound; 1878.21 cm^{-1} and 2000.00 cm^{-1} to weak, overtone C-H bending of aromatic compound; 2374.66 cm^{-1} to strong O=C=O stretching of carbon dioxide; 2859.80 cm^{-1} and 2926.54 cm^{-1} to strong, broad N-H stretching of amine salt; 3436.00 cm^{-1} to strong, broad intermolecular bonded O-H stretching of alcohols and 3757.00 cm^{-1} to medium, sharp and free O-H stretching of alcohols [22].

The synthesized AgNPs with *C. siamea* leaf extract show varying intensities of transmittance at 3868.00 cm^{-1}, 3752.23 cm^{-1}, 3445.00 cm^{-1}, 2927.76 cm^{-1}, 2375.83 cm^{-1}, 1997.76 cm^{-1}, 1877.00 cm^{-1}, 1631.73 cm^{-1}, 1056.00 cm^{-1}, 780.48 cm^{-1}, and 685.36 cm^{-1} due to the interaction between metal ions and the biocompounds present in *C. siamea* leaves [23]. The transmittance at 685.36 cm^{-1} is associated with the strong C=C bending of the disubstituted alkane compound, the medium C=C bending of the trisubstituted alkane compound, and the medium C-N stretching of the amine molecule, respectively, at 780.48 cm^{-1}. Additionally, the peaks at 1877.00 cm^{-1} and 1997.76 cm^{-1} indicate the weak, overtone C-H bending of the aromatic compound, and the peak at

1631.73 cm^{-1} represents the mild C=C stretching of the conjugated alkene molecule. This could be because ether or ester groups are covalently linked to the nanoparticle [23]. 3752.23 cm^{-1} and 3868.00 cm^{-1} represent medium, sharp, and free O-H stretching of alcohols; 2927.76 cm^{-1} represents strong, broad O-H stretching of carboxylic acid; 3445.00 cm^{-1} represents strong, broad intermolecular bonded O-H stretching of alcohols; and 2375.83 cm^{-1} represents strong O=C=O stretching of carbon dioxide [24]. Furthermore, the infrared bands 683.13 cm^{-1} to 685.36 cm^{-1}, 778.34 cm^{-1} to 780.48 cm^{-1}, 1054.09 cm^{-1} to 1056.00 cm^{-1}, 1630.66 cm^{-1} to 1631.73 cm^{-1}, 1878.21 cm^{-1} to 1877.00 cm^{-1}, 2000.00 cm^{-1} to 1997.76 cm^{-1}, 2374.66 cm^{-1} to 2375.83 cm^{-1}, 2859.80 cm^{-1} to 2927.76 cm^{-1}, 3436.00 cm^{-1} to 3445.00 cm^{-1}, and 3757.00 cm^{-1} to 3752.23 cm^{-1} are also altered. These alterations might be due to interactions among molecules, which indicate changes in the molecular structures of Ag and the extract, as well as due to chemical reactions, which led to the modification of the nanoparticle. By comparing the infrared spectra of the two substances, it was also possible to identify the presence of different absorption bands of phytoconstituents of *C. siamea* leaf extract in the AgNPs. These bands show that AgNPs bind to carboxylate groups of alcohol and proteins [24]. Furthermore, the IR band at 2926.54 cm^{-1} entirely disappeared, while a new band at 3868.00 cm^{-1} emerged. This could be because the various functional groups may have contributed to the synthesis of the nanoparticles [24].

The bio-organic phase on the surface of the Ag salt has crystallized because of the stabilizing effect of each of these functional groups in the *C. siamea* leaf extract and their reduction to AgNPs. It is well known that interactions between metal salts and functional groups present in biological components promote the formation of nanoparticles [25]. Therefore, the potential functional groups in charge of stabilizing and capping the produced AgNPs were determined using the FTIR data. The FTIR absorption values of the extract and the synthesized nanoparticle are shown in **Table 2**.

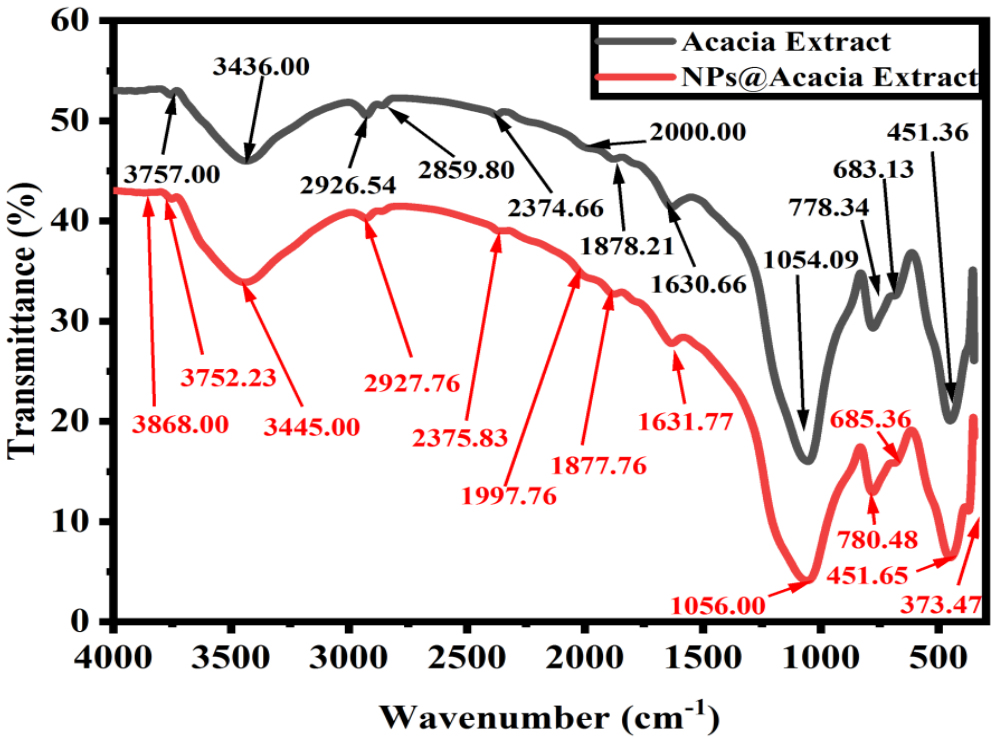

Figure 6: FTIR analysis of *C. siamea* leaf extract and the synthesized AgNPs

Table 2: The FTIR absorption values of the extract and the synthesized nanoparticle

Wave number (cm^{-1})	*C. siamea* leaf extract	AgNPs@ *C. siamea* leaf extract	Functional group
4000-3000	3757, 3436,	3868, 3752, 3445	O-H (stretching)
3000-2500	2927, 2860	2928	C-H (stretching)

2400-2000	2375, 2000	2376	O=C=O (stretching)
2000-1650	1878	1998, 1877	C-H (bending)
1650-1600	1631	1632	C=C (stretching)
1600-1300	-	-	N-O (stretching)
1300-1000	1054	1056	O-H (bending)
1000-650	778, 683	780, 685	C=C (bending)

3.3. Structural Studies of Ag/TiO_2 Nanostructures

The XRD pattern of the green-synthesized AgNPs was carried out to confirm the phase development on the synthesized sample, as shown in **Fig. 7a**, which shows the prominent peaks at (2θ degrees) 38.46, 46.41, 55.06, 57.70, 64.94, 67.77, 75.00, and 77.30. The (111), (200), (211), (210), (211), (220), (220), and (311) planes are represented by these points, respectively. When the AgNPs index was generated, it was discovered that the pattern had a face-centered cubic (FCC) shape using the JCPDS card (file no.: #030931) [26]. The Scherer equation was used to estimate the average crystallite size of the synthesized nanoparticle to determine its crystalline nature [27]. The calculated average of crystallite size was 3.95 nm [28]. It was evident that Ag had a significant role in the biosynthesis of the stronger planes. Similar findings were reported by previous researchers for AgNPs [29]. **Fig. 7b & c** displays the XRD patterns of the TiO_2 and TiO_2 incorporated with AgNPs using an extract from *C. siamea* leaves. As illustrated in **Fig. 7b**, the TiO_2 is made up of a combination of rutile and anatase phases in line with the JCPDS reference pattern on card number #83-2243. The observed peaks at the 2θ (degrees) values of 25.67, 38.92, 48.38, 68.72, 70.92, and 76.33, respectively, indicate the anatase phase of TiO_2 and are caused by the (101), (112), (200), (116), (220), and (301) crystallographic planes. Nonetheless, the peaks at 2θ (degrees) of 54.21 and 63.00 are attributed to the (105) and (204) crystallographic planes and are consistent with the rutile phase of TiO_2. The material exhibited a crystalline body-centered tetragonal structure with an average crystallite size of 7.47 nm. Upon incorporation of synthesized AgNPs into TiO_2, the structure remained crystalline but changed to a face-centered cubic (FCC) structure, with a reduced average crystallite size of 4.53 nm, as shown in **Fig. 7c**. This significantly fits the JCPDS reference pattern, card number #21-1276. The rutile phase of the TiO_2 and the peaks formed by the AgNPs in the nanoparticle nearly overlap. The same peaks in the TiO_2 nanocomposite indicate that the AgNPs were successfully doped into the TiO_2. The sample's crystallite size significantly shrank, suggesting that the TiO_2 photoanode improved in efficiency and would be a good fit for solar cell production [30].

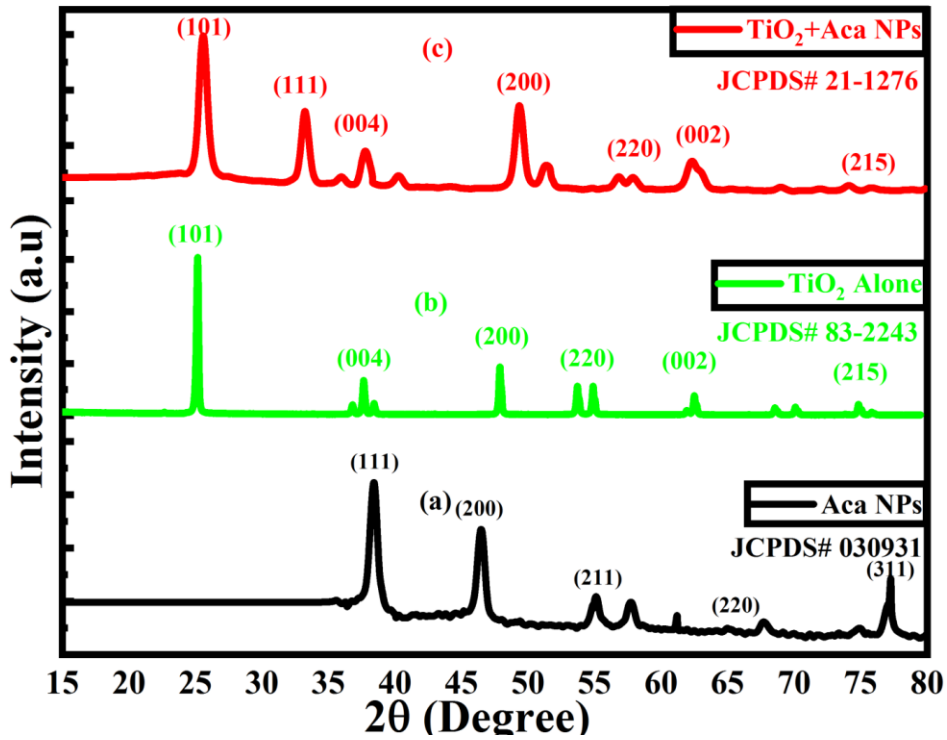

Figure 7: XRD patterns of (**a**) Synthesized AgNPs, (**b**) TiO_2 alone, (**c**) TiO_2 incorporated with the synthesized AgNPs

As the crystallite size decreases, AgNPs' specific surface area increases. This is due to the fact that a material's total surface area is proportional to the cube of its particle size, whereas its mass is related to its volume, which is less affected by particle size. Because they can interact with their surroundings more effectively, nanoparticles having a larger specific surface area are more beneficial in applications like DSSC. In quantum physics, particles of nanometer-scale dimensions experience unique phenomena such as the quantum size effect. AgNPs' electrical properties may be altered by these actions, perhaps leading to better optical and catalytic properties [31]. Quantum size effect is also responsible for the surface-enhanced Raman scattering observed in AgNPs, which has applications in spectrum detection. AgNPs' incredibly small crystallite sizes also affect their stability and dispersibility. Because of their propensity to agglomerate, Ag particles in bulk materials are less suitable for applications where dispersion in a liquid or gas environment is required. AgNPs' unique properties are ensured to be retained in a useful form by their smaller crystallite sizes, which enable them to scatter more easily without clumping together. These particles can increase DSSC reaction speeds and efficiency by providing more active areas for chemical reactions [31].

3.4. Morphological Studies of Ag/TiO_2 Nanostructures

Fig. 8 a & b display the SEM micrographs of TiO_2 and TiO_2 coupled with AgNPs produced from *C. siamea* leaf extract. The SEM micrograph of the TiO_2 nanoparticle shows the formation of a permeable structure, as shown in **Fig. 8a**. The nanoparticle addition changed the sample's surface morphology and resulted in a more spherical shape of the TiO_2 adjusted with the nanoparticle, as shown in **Fig. 8b**. There were no prominent areas of aggregated particles, and the apparent morphology was uniformly packed. According to the literature, spherical nanoparticles have a high surface area relative to their volume, which makes them useful for applications like catalysis and sensing. They exhibit SPR, this makes them viable in DSSC applications. They also ensure uniformity in properties and behavior and can exhibit enhanced optical properties, such as increased absorption and scattering. [32].

The EDS assessment of the TiO_2 nanoparticles in **Fig. 8c** demonstrated that the particles were pure TiO_2 and verified that they were made of titanium and oxygen. As seen in **Fig. 8d**, the EDS result for the TiO_2 nanocomposite validates the existence of Ti, O, and Ag. The presence of the nanoparticles was verified by the observed distinctive peak of Ag.

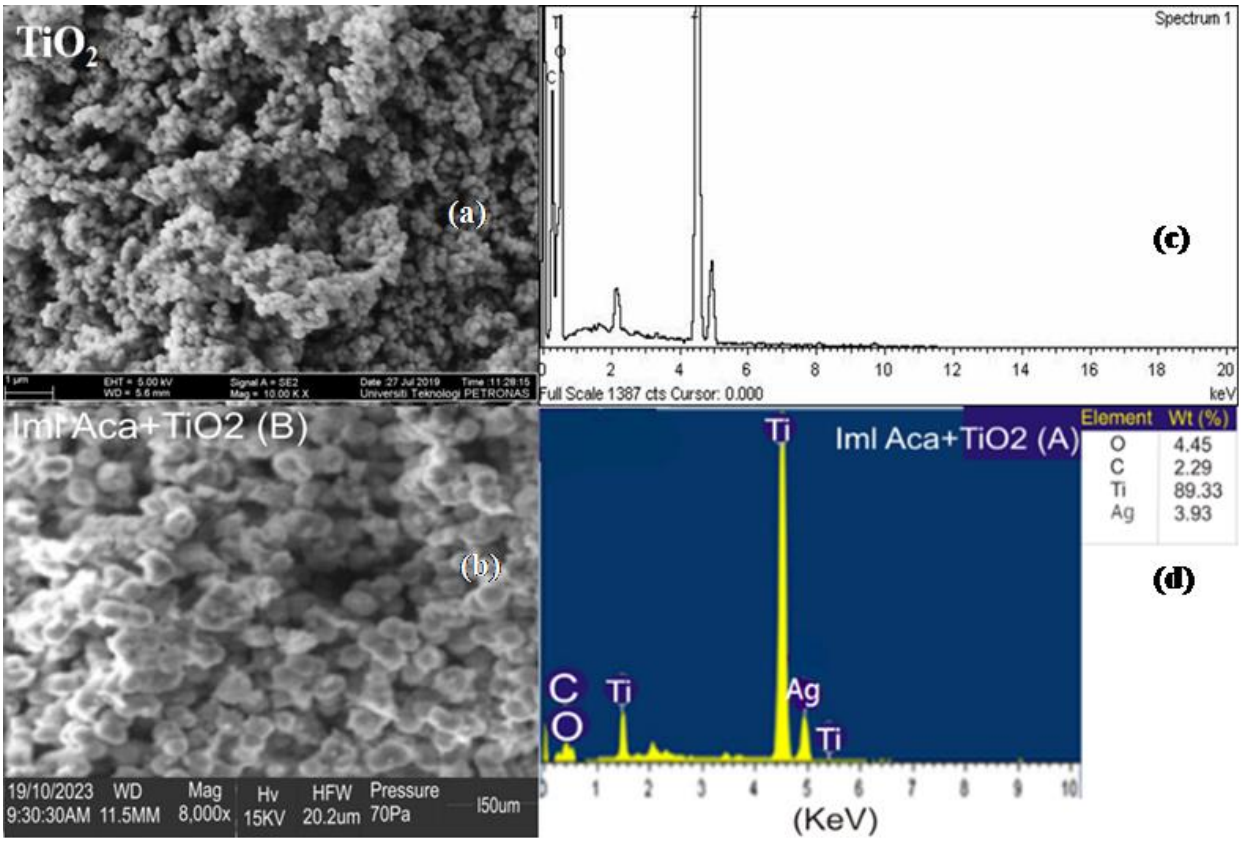

Figure 8: (**a**) SEM micrograph of TiO_2, (**b**) SEM micrograph of TiO_2 incorporated with the synthesized AgNPs, (**c**) EDS result of the TiO_2 nanoparticles, (**d**) EDS result for the TiO_2 nanocomposite

TEM characterization of the Ag/TiO_2 nanocomposite, TiO_2, and nanoparticle were performed to bolster the structural characterization. **Fig. 9a** shows the TEM picture of the AgNPs made with a *C. siamea* leaf extract. According to the TEM micrograph in **Fig. 9a**, the nanoparticle is spherical and has a broad size range between 3 and 8 nm, with a significant portion of the particles falling between 4 and 6 nm. Based on the size distribution histogram in **Fig. 9b**, the TEM micrograph also verifies the creation of nanoparticles with a size average of 4.85 nm. Literature suggests that increasing the surface area of TiO_2 is important to improve its light absorption, and that this surface area is proportional to the size of the nanoparticle [33]. As the size of a nanoparticle shrinks, its surface area increases, increasing the possibility of collisions and quickening the pace of reaction [30]. According to the TEM image in **Fig. 9c**, the TiO_2 nanoparticle has a spherical shape and ranges greatly in size from 2 to 22 nm. Furthermore, as the size distribution histogram in **Fig. 9d** illustrates, the TEM micrograph validates the creation of nanoparticles with a size average of 7.98 nm.

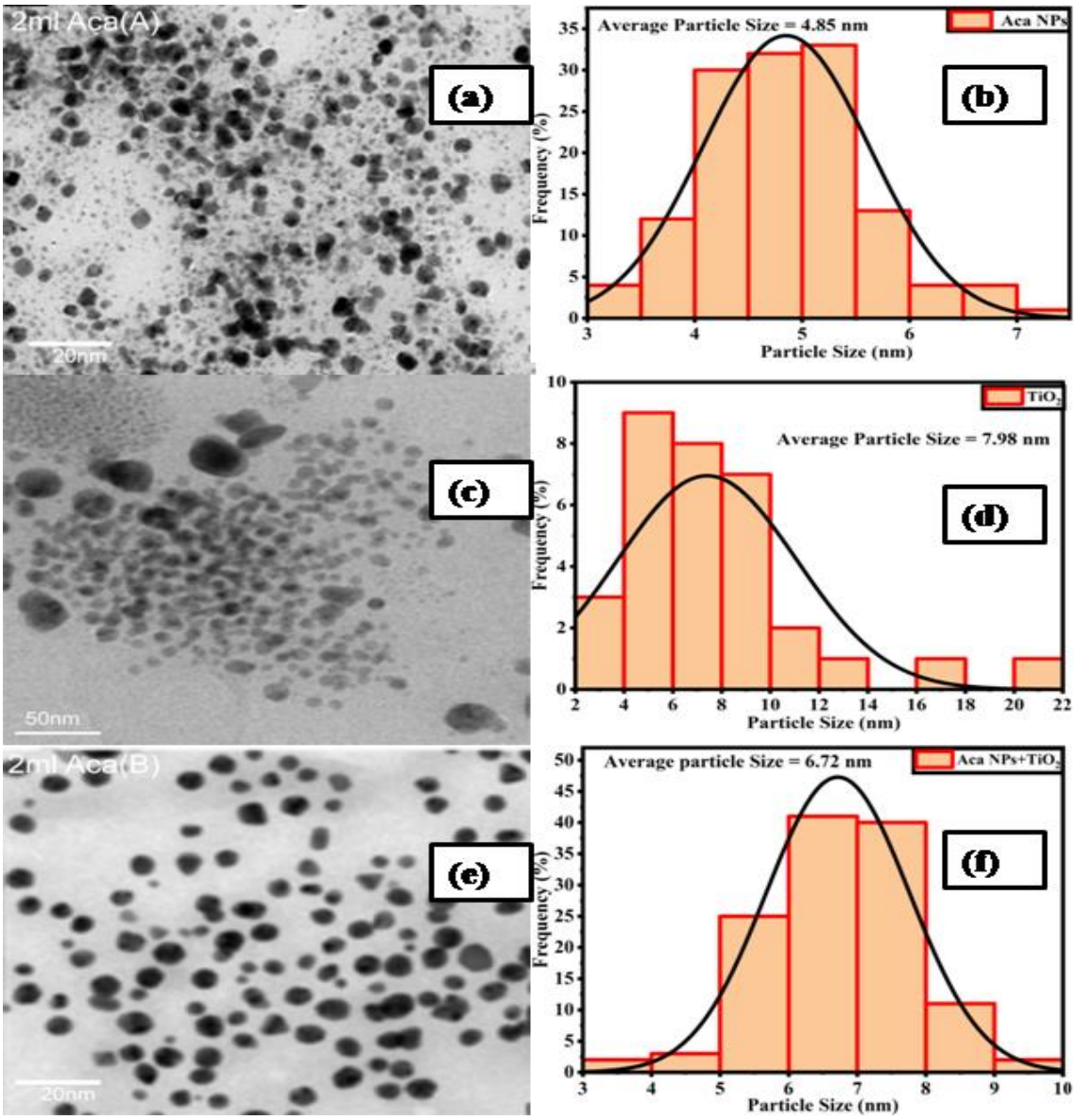

Figure 9: (**a**) TEM image of the synthesized AgNPs, (**b**) Corresponding size distribution histogram of the synthesized AgNPs, (**c**) TEM image of TiO_2 alone, (**d**) Corresponding size distribution histogram of TiO_2, (**e**)TEM image of TiO_2 incorporated with the synthesized AgNPs, (**f**) Corresponding size distribution histogram of TiO_2 incorporated with the synthesized AgNPs.

Fig. 9e shows the TEM picture of the TiO_2 mixed with the synthesized AgNPs, which illustrates that the nanoparticle is spherical and has a broad size range between 3 and 10 nm, with a significant portion of the particles falling between 5 and 9 nm. Furthermore, the size distribution histogram in **Fig. 9f** indicates that the TEM micrograph validates the creation of nanoparticles with an average size of 6.72 nm. Ag/TiO_2 nanocomposites' behavior is considerably changed by particle size reduction since it modifies surface area, dispersion, electrical properties, and catalytic performance, all of which can be employed to increase the particles' performance in DSSC and other applications [34].

3.5. Electrical Characterization Ag/TiO_2 Thin Films

The electrical characteristics of the TiO_2 film and the modified TiO_2 film were examined using the four-point probe. This method suited significantly with materials that have a consistent current density throughout. The method was applied to determine the samples' conductivity, resistivity, and resistance [35, 36]. The films' cross-

sectional area (A) was 9.75 cm^2, and their length (L) between the probes was 6.5 cm. The resistivity (ρ) was calculated in terms of open circuit voltage (V_{oc}) and short circuit current (I_{sc}) using **Eq. (1)**; while the resistance (R) was estimated by **Eq. (2)**. Conductivity (σ) was given as the reciprocal of resistivity [35].

$$\rho = \frac{\pi}{ln2} \cdot \frac{V_{oc}}{I_{sc}} \quad (1)$$

$$R = \frac{\rho L}{A} \quad (2)$$

The voltage and current density graphs for the TiO_2 and modified TiO_2 films are displayed in **Fig. 10**. Additionally, **Table 3** contains a summary of the electrical parameters for films and modified films. As shown in **Fig. 10** and **Table 3**, the TiO_2 film exhibited a current of 1.81 µA and a voltage of 0.53 V. With the incorporation of synthesized AgNPs, the current increased to 3.18 µA and the voltage to 0.56 V. The addition of AgNPs significantly reduced the resistance and resistivity, thereby enhancing conductivity, electrical performance, and electron mobility [35, 36].

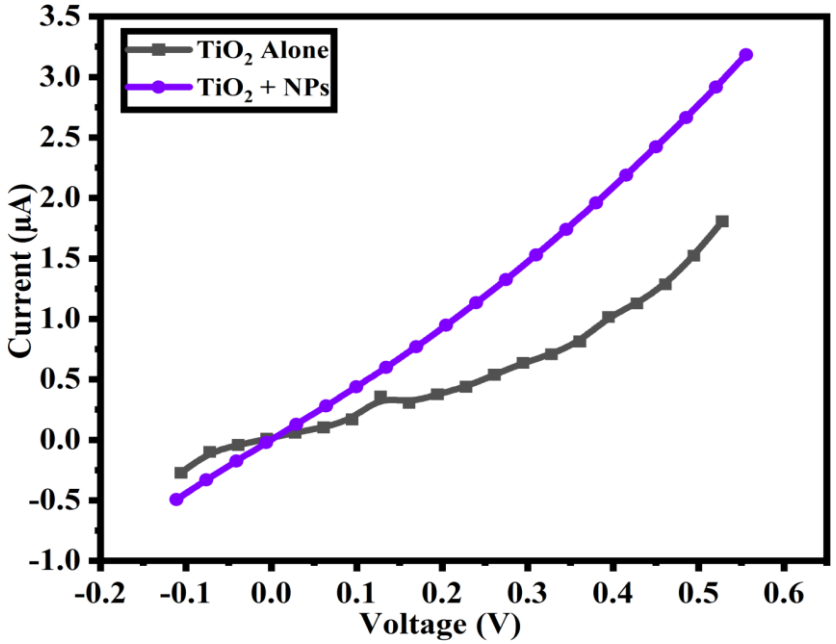

Figure 10: Graphs of current versus voltage for TiO_2 and modified TiO_2 films.

AgNPs create a percolative network when they are introduced to TiO_2 films. Individual particles become interconnected as a result, allowing unhindered electron movement and increasing overall conductivity. According to the percolation theory, a continuous conductive channel forms when a critical concentration of Ag particles is reached, resulting in a notable increase in conductivity. Additionally, a characteristic of AgNPs known as SPR adds to their enhanced conductivity. An electrical signal is magnified when light strikes the film's surface because the electromagnetic waves stimulate the Ag particles' free electrons. Increasing conductivity improves the films' ability to transport electrical signals. Moreover, Ag particles create a solid connection with the TiO_2 surface as they are integrated into the film layer. A larger conductivity is the outcome of this bonding's enhanced ability to transmit electrical charges [35, 36]. The development of the Ag/TiO_2 interface between the two materials also leads to an improvement in the conductivity. The bulk conduction of the film, which penetrates the entire material rather than just the surface, is where the increase in conductivity is primarily observed. The implication that the film may effectively carry electricity without relying on a surface layer makes this noteworthy [35, 36].

Table 3: Summary of the electrical characteristics of TiO_2 and modified TiO_2 films

Sample	TiO_2 film	TiO_2 film+Aca AgNPs
Length between probes (cm)	6.5	6.5

Area of film (cm^2)	9.75	9.75
Currently, I (μA)	1.81	3.18
Voltage, V (V)	0.53	0.56
Resistance, R (Ω)	8.85×10^5	5.32×10^5
Resistivity, ρ (Ω.m)	13.27×10^5	7.98×10^5
Conductivity, σ (S/m)	7.53×10^{-7}	1.25×10^{-6}

4. Conclusion

The synergistic effect of the green-synthesized Ag/TiO_2 nanocomposite was illustrated using a leaf extract from *C. siamea*. The absorbance spectral analysis revealed that just 2 mL of the extract was enough for nanoparticles synthesis, with the highest peak at around 425 nm. The absorbance was improved by the nanoparticle's interaction with TiO_2. It was shown that when absorbance increased, the energy gap decreased. The presence of many functional groups, which potentially contribute to the nanoparticle's formation, was revealed by the FTIR study results. The synthesized nanoparticle was also found to be crystalline, with an average crystallite size of 3.95 nm, according to XRD results. The morphology of the nanoparticle exhibited that it was uniformly distributed and well-formed. When coupled with the nanoparticle, the TiO_2 surface became smoother and more spherical. EDS of the TiO_2 nanoparticle and TiO_2 nanocomposite verified the existence of Ag and other chemical components. The creation of nanoparticles and nanocomposites with average sizes of 4.85 nm and 6.92 nm, respectively, was further confirmed by the evaluation of the particles' TEM micrographs. The electrical properties of films and modified films showed that the calculated resistance and resistivity significantly decreased when the films were incorporated with AgNPs. As a result, the addition of AgNPs increased conductivity by 60.24%, which enhanced electron mobility and electrical properties. The improved conductivity of the TiO_2 films combined with the AgNPs and the interaction between TiO_2 and Ag has demonstrated promising characteristics and might be suggested for application in DSSC.

Acknowledgment

The authors thank the Engineering Materials and Development Institute at Ondo State University in Akure, Nigeria, for the film analyses and IV characterization, and the Department of Pure and Applied Physics at LAUTECH, Nigeria, for the UV-vis analysis. Additionally, O. A. thanks TETFUND for 2024 Institution Based Research (IBR) fund, LAUTECH, Nigeria, for the support received.

Conflict of Interest

The authors declare that they have no conflict of interest.

References

[1] O. Adedokun, G. A. Alamu and Y. K. Sanusi, "Optical studies of natural dyes and green synthesized silver nanoparticles embedded in titanium (iv) oxide for application in dye sensitized solar cells,"*Science Focus: An International Journal of Biological and Physical Sciences*,Vol. 23, no. 2, pp.22-31, 2018.

[2] G. A. Alamu, O. Adedokun, I. T. Bello and Y. K. Sanusi, "Plasmonic enhancement of visible light absorption in Ag-TiO_2 based dye-sensitized solar cells," Chemical *Physics Impact,* Vol.12, p. 100037, 2021.

[3] I. Benammar, R. Salhi, J. -L. Deschanvres and R. Maalej, "Study of the physico-chemical properties of sol-gel (Er, Yb) doped TiO2 nanoparticles prepared with a novel protocol," *Journal of Applied Sciences and Nanotechnology*, vol. 3 (2), P. 1-17, 2023.

[4] O. Adedokun, T. Kamil and A. O. Awodugba, "Review on natural dye-sensitized solar cells," International *Journal of Engineering Technologies,* vol. 2, no. 2, 2016.

[5] Z. S. Ghazi, M. R. Mohammad, M. A. Abbood and A. A. Hussein, "Antibacterial studying of silver nanoparticles synthesized by chemical reduction method using different stabilized concentrations," *Journal of Applied Sciences and Nanotechnology,* vol. 2, (3), P. 106-114, 2022.

[6] M. T. Hamid, N. N. Hussein, G. M. Sulaiman, *et al.,* "Antibacterial and antibiofilm properties of silver nanoparticles synthesized using *Carthamus tinctorius* extract against various multidrug resistant bacterial strains," *Discovery Applied Science* **7**, p. 548, 2025.

[7] A. Muhammad, Y. Riffat, A. Rizwan, A. Ana, M. Madiha and U. Shehla, "Green synthesis of silver nanoparticles (AgNPs), structural characterization and their antibacterial potentials, "National Centre for Biotechnology Information, vol. 20, no. 2, 2022.

[8] J. Joud, A. Wassim, K. Adawia and A. Rawaa, "Green synthesis of silver nanoparticles using aqueous extract of Acacia cyanophylla and its antibacterial activity,"National Centre for Biotechnology Information, vol. 7, no. 9, p. e08033, 2021.

[9] C. N. Nkanyiso, K. B. Albertus, G. N. Zuzingcebo, G. D. Nkosinathi and V. P. Rajasekhar, "Green synthesis, characterization and application of silver nanoparticles using bioflocculant: A review," Bioengineering (Basel), vol. 11, no. 5, p. 492, 2024.

[10] M. M. Sasi, S. O. Hribesh, R. O. Eshkourfu, and R. O. Amara, "Biosynthesis of silver nanoparticles using ajucaive leaf extract and assessment of their activity on E. coli and streptococcus bacteria," European Scientific Journal, ESJ, vol. 37, p. 373, 2025.

[11] A. Chahardoli, F. Qalekhani, P. Hajmomeni, Y. Shokoohinia and A. Fattahi, "Enhanced hemocompatibility, antimicrobial and anti-inflammatory properties of biomolecules stabilized AgNPs with cytotoxic effects on cancer cells," *Scientific Reports*, vol. 15, p. 1186, 2025.

[12] K. Murugan, B. Senthilkumar, D. Senbagam and S. Al-Sohaibani, "Biosynthesis of silver nanoparticles using *Acacia leucophloea* extract and their antibacterial activity," *International Journal of Nanomedicine*, vol. 9, p. 2431-8, 2014.

[13] O. U. Edwina, P. K. Abidemi, M. Sixberth and R. Neerish, "Bioinspired synthesis of *Acacia senegal* leaf extract functionalized silver nanoparticles and its antimicrobial evaluation," *Journal of Nanomaterials*, 2020.

[14] S. A. Nuha, S. B. Ramesa, A. A. Sabah, M. E. Doaa, M. A. Hussah and H. D. Maha, "Anticancer and antimicrobial activity of silver nanoparticles synthesized from pods of *Acacia nilotica," Processes*, vol. *11, no.* 2, p.301, 2023.

[15] N. H. Ibrahim, G. M. Taha, N. S. A. Hagaggi and A. M. Marwa, "Green synthesis of silver nanoparticles and its environmental sensor ability to some heavy metals," *BMC Chemistry* vol. 18, p. 7, 2024.

[16] O. Adedokun, M. K. Awodele, Y. K. Sanusi and A. O. Awodugba, "Natural dye extracts from fruit peels as sensitizers in ZnO-based dye-sensitized solar cells," *IOP Conf. Ser.*: *Earth Environmental Science,* vol. 173, p. 012040, 2018.

[17] S. C. G. Kiruba Daniel, G. Vinothini, N. Subramanian, K. Nehru and M. Sivakumar, "Biosynthesis of Cu, ZVI, and Ag nanoparticles using D*odonaea viscosa* extract for antibacterial activity against human pathogens," *Journal of Nanoparticle Research*, vol. 15, no. 1, p. 1319, 2013.

[18] A. Y. Obaid, S. A. Al-Thabaiti, L. M. Al-Harbi and Z. Khan, "Extracellular bio-synthesis of silver nanoparticles," Global *Advanced Research Journal of Microbiology,* vol. 3, no. 8, p. 119-126, 2015.

[19] A. Yardily and N. Sunitha, "Green synthesis of iron nanoparticles using hibiscus leaf extract, characterization, antimicrobial activity," *International Journal of Scientific Research and Revie*w, vol. 8, no. 7, 2019.

[20] S. Ito, T. N. Murakami, P. Comte, P. Liska, C. Grätzel, M. K. Nazeeruddin and M. Grätzel, "Fabrication of thin film dye sensitized solar cells with solar to electric power conversion efficiency over 10%," Thin *Solid Films,* Vol.516, No. 14, p. 4613-4619, 2008.

[21] P. Levchuk, M. Sillanpää, C. Guillard, D. Gregori, D. Chateau, F. Chaput, F. Lerouge and S. Parola, "Enhanced photocatalytic activity through insertion of plasmonic nanostructures into porous TiO_2/SiO_2 hybrid composite films,"*Journal of Catalysis,* vol. 342,p. 117-124, 2016.

[22] M. F. Zayed, W. H. Eisa and A. A. Shabaka, "Malva parviflora extract assisted green synthesis of silver nanoparticles," *Spectrochim. Acta A,* vol. 98, p. 423–428, 2012.

[23] Y. P. Yew, K. Shameli and M. Miyake, "Green synthesis of magnetite (Fe_3O_4) nanoparticles using seaweed (*Kappaphycusalvarezii*) extract," *Nanoscale Research Letters,* vol. 11, p. 1–7, 2016.

[24] I. H. Kim, E. J. Park, C. H. Park, S. H. Han, H. O. Seo and Y. D. Kim, *Catalysis Today*, vol. 295, p. 54–64, 2017.

[25] M. M. Ganesh Babu and P. Gunasekaran, "Production and structural characterization of crystalline silver nanoparticles from *Bacillus cereus* isolate," *Colloids Surface B,* vol. 74, p. 191–195, 2009.

[26] S. Shukla, A. Jadaun, V. Arora, R. K. Sinha, N. Biyani and V. Jain, "In vitro toxicity assessment of chitosan oligosaccharide-coated iron oxide nanoparticles," *Toxicology Reports,* vol. 2, p. 27–39, 2015.

[27] B. Ajitha, Y. Ashok Kumar Reddy, P. S. Reddy, "Biogenic nano-scale silver particles by *Tephrosia purpurea* leaf extract and their inborn antimicrobial activity," *Spectrochim. Acta Part A Molecular Biomolecular Spectroscopy*, vol. 121, p. 164–172, 2014.

[28] Y. C. Chang and D. H. Chen, "Preparation and adsorption properties of monodispersed chitosan-bound Fe_3O_4 magnetic nanoparticles for removal of Cu(II) ions," *Journal of Colloid and Interface Science*, vol. 283, p. 446–51, 2005.

[29] N. Basavegowda, A. Idhayadhulla and Y. R. Lee, "Preparation of Au and Ag nanoparticles using *Artemisia annua* and their in vitro antibacterial and tyrosinase inhibitory activities," *Material Science and Engineering C*, vol. 43, p. 56–64, 2014.

[30] C. P. Devatha, K. Jagadeesh and P. Mallikarjun, "Effect of green-synthesized iron nanoparticles by *Azardirachta Indica* in different proportions on antibacterial activity,"*Environmental Nanotechnology, Monitoring & Management*, vol. 9, p. 85-94, 2018.

[31] D. B. Dupare, "Synthesis and characterization of silver nanoparticle by *Zingiber officinale* extract and their antibacterial activity," *International Journal of Advanced Research, Communication and Technology*, vol. 12, p. 4, 2021.

[32] J. Zhang, M. Ahmadi, G. Fargas, N. Perinka, J. Reguera, S. Lanceros-Méndez, L. Llanes and E. Jiménez-Piqu, "Silver nanoparticles for conductive inks: from synthesis and ink formulation to their use in printing technologies," Metals, vol. 12, p. 234, 2022.

[33] H. J. Huang, J. Sung-Jun, A. PSupriya and Hak-Sung Kim, "Efficiency enhancement in dye-sensitized solar cells using the shape/size dependent plasmonic nanocomposite photoanodes incorporating silver nanoparticles, *Nanoscale*, vol. 9**,** 7960-7969, 2017.

[34] P. Sarkar, S. Panda, B. Maji and A. K. Mukhopadhyay, "Comparative study of Au and Ag nanoparticle to improved in absorption in plasmonic solar cell," *Devices for Integrated Circuit (DevIC), Kalyani, India*, p. 175-179, 2017.

[35] M. I. Khan, K. A. Bhatti, R. Qindeel, L. G. Bousiakou, N. Alonizanand Fazal-e-Aleem, "Investigations of the structural, morphological and electrical properties of multilayer ZnO/TiO_2 thin films, deposited by sol–gel technique," *Results in Physics*, vol. 6, p. 156–160, 2016.

[36] A. S. Jasim and O. N. Salman, "The effect of solvent variation on structural, optical, and electrical properties of TiO_2 films prepared by hydrothermal method," *Journal of Applied Sciences and Nanotechnology*, vol. 3 (2), P. 59-69, 2023.